AGU PUBLICATIONS

JGR

Journal of Geophysical Research: Solid Earth

RESEARCH ARTICLE
10.1002/2017JB015193

Key Points:
- In homogeneous titanomagnetites of a range of compositions, Curie temperatures change strongly and reversibly as a result of thermal treatments
- These changes are due to reversible reordering of the distribution of cations and/or vacancies
- Low-temperature complex susceptibility and high-temperature hysteresis behavior are also strongly affected by annealing and quenching

Supporting Information:
- Supporting Information S1
- Data Set S1

Correspondence to:
M. Jackson,
jacks057@umn.edu

Citation:
Jackson, M., & Bowles, J. (2018). Malleable Curie temperatures of natural titanomagnetites: Occurrences, modes, and mechanisms. *Journal of Geophysical Research: Solid Earth*, *123*. https://doi.org/10.1002/2017JB015193

Received 2 NOV 2017
Accepted 19 JAN 2018
Accepted article online 24 JAN 2018

Malleable Curie Temperatures of Natural Titanomagnetites: Occurrences, Modes, and Mechanisms

Mike Jackson[1] **and Julie Bowles**[2]

[1]Institute for Rock Magnetism, Department of Earth Sciences, University of Minnesota, Twin Cities, Minneapolis, MN, USA, [2]Department of Geosciences, University of Wisconsin-Milwaukee, Milwaukee, WI, USA

Abstract Intermediate-composition titanomagnetites have Curie temperatures (T_c) that depend not only on composition but also on thermal history, with increases of 100°C or more in T_c produced by moderate-temperature (300–400°C) annealing in the laboratory or in slow natural cooling and comparable decreases produced by more rapid cooling ("quenching") from higher temperatures. New samples spanning a range of titanomagnetite compositions exhibit reversible changes in T_c comparable to those previously documented for pyroclastic samples from Mt. St. Helens and Novarupta. Additional high- and low-temperature measurements help to shed light on the nanoscale mechanisms responsible for the observed changes in T_c. High-T hysteresis measurements exhibit a peak in high-field slope $k_{hf}(T)$ at the Curie temperature, and the peak magnitude decreases as T_c increases with annealing. Sharp changes in low-T magnetic behavior are also strongly affected by prior annealing or quenching, suggesting that these treatments affect the intrasite cation distributions. We have examined the effects of oxidation state and nonstoichiometry on the magnitude of T_c changes produced by quenching/annealing in different atmospheres. Treatments in air generally cause large changes ($\Delta T_c > 100°$). In an inert atmosphere, the changes are similar in many samples but strongly diminished in others. When the samples are embedded in a reducing material, ΔT_c becomes insignificant. These results strongly suggest that cation vacancies play an essential role in the cation rearrangements responsible for the observed changes in T_c. Some form of octahedral-site chemical clustering or short-range ordering appears to be the best way to explain the large observed changes in T_c.

1. Introduction

Through their natural remanent magnetizations (NRMs) and their physical/chemical characteristics, titanomagnetites (minerals of the magnetite-ulvöspinel solid solution series, $Fe_{3-x}Ti_xO_4$ ($0 \le x \le 1$), here abbreviated as TM) provide key information on a wide range of natural phenomena. Paleomagnetic, rock-magnetic, and environmental-magnetic studies of TM-bearing natural materials document the past behavior and evolution of the geomagnetic field, tectonic plate motions, and geological processes that imprint and overprint NRMs, as well as varying surficial environmental conditions (e.g., Evans & Heller, 2003; Merrill & McElhinny, 1983). Despite many years of study, enduring mysteries remain about TM magnetic behavior, including changes in their fundamental properties resulting from quenching or annealing under different redox conditions, in the laboratory and in nature (e.g., Bowles et al., 2013; Jackson & Bowles, 2014; Lattard et al., 2006; Moskowitz, 1987; Stephenson, 1969; Wanamaker & Moskowitz, 1994).

The fundamental mineral magnetism of the titanomagnetites is controlled by superexchange coupling of iron cations that occupy tetrahedral (A) and octahedral (B) sites within the inverse-spinel crystal-chemical structure (e.g., Dunlop & Özdemir, 1997; Néel, 1955). In TMs and other spinel ferrites, this coupling produces a ferrimagnetically ordered state, with a net spontaneous magnetization due to the imbalance of the antiparallel moments of the A and B sublattices. The strength of the spontaneous magnetization M_s, as well as its temperature dependence, is related to the spatial arrangement of magnetic and nonmagnetic cations and vacancies, and to the geometry of the superexchange links (e.g., Néel, 1955; O'Reilly & Banerjee, 1965). In end-member magnetite ($x = 0$) with the ideal inverse-spinel cation arrangement, the A sites contain Fe^{3+} and the B sites contain equal proportions of Fe^{2+} and Fe^{3+}; this arrangement is denoted by the structural formula $Fe^{3+}[Fe^{2+}\ Fe^{3+}]O_4$. Titanium is accommodated by the paired substitution $Ti^{4+} + Fe^{2+} \leftrightarrow 2Fe^{3+}$, and it is generally believed to reside entirely in B sites (Wechsler et al., 1984). With the addition of Ti, the ferrous-ferric cation site distribution necessarily changes, and different models have been proposed to

account for $M_s(x)$ and other data (e.g., Akimoto, 1954; Néel, 1955; O'Reilly & Banerjee, 1965). For example, in the Néel model, the substitution involves only B-site cations for $x \leq 0.5$ (Fe^{3+} [Fe^{2+}_{1+x} Fe^{3+}_{1-2x} Ti^{4+}_{x}] O^{2-}_{4}), preserving as far as possible the inverse ferrous-ferric ordering, whereas the more disordered Akimoto model consumes A- and B-site ferric ions at the same rate, resulting in mixed valence states in both sites (Fe^{3+}_{1-x} Fe^{2+}_{x} [Fe^{2+} Fe^{3+}_{1-x} Ti^{4+}_{x}] O^{2-}_{4}). These models predict different trends for Curie temperature $T_c(x)$ as well as for $M_s(x)$ (Moskowitz, 1987; Stephenson, 1972b). Other models (e.g., Kakol, Sabol, & Honig, 1991; O'Reilly & Banerjee, 1965) lie between these two in their predicted properties.

Other cations, especially Al^{3+} and Mg^{2+}, are common substitutes in titanomagnetites, generally occurring preferentially in B sites (e.g., Creer & Stephenson, 1972), and like Ti^{4+}, they cause a decrease in both M_s and T_c. Furthermore, oxidation commonly produces cation-deficient titanomagnetites by several mechanisms, significantly affecting their magnetic properties (Hauptman, 1974; Readman & O'Reilly, 1972; Stephenson, 1972a). Charge balance dictates the paired substitution $3Fe^{2+} \leftrightarrow 2Fe^{3+} + \square$, that is, ferrous ions are replaced by vacancies and ferric ions. Vacancies also occur preferentially in the octahedral sites, and their presence diminishes M_s but increases T_c (e.g., Hauptman, 1974; Lattard et al., 2006; Wanamaker & Moskowitz, 1994).

In "homogeneous" titanomagnetites, Ti cations and vacancies are located randomly in B sites throughout the crystal lattice, so there is necessarily some fine-scale heterogeneity, but because of the multiply connected network of superexchange links, long-range magnetic order predominates and these bulk materials behave homogeneously (e.g., a given composition has a single Curie temperature). Homogeneous phases over the entire compositional range $0 \leq x \leq 1$ are thermodynamically stable at sufficiently high temperature, but below a solvus, intermediate-composition TMs become unstable or metastable. In this miscibility gap, unmixing of TM into Ti-rich and Ti-poor cubic-phase intergrowths is thermodynamically favored but limited by temperature-dependent diffusion rates (e.g., Bowles et al., 2013; Price, 1981, 1982). Rapid cooling allows preservation of homogeneous intermediate-composition TMs in some volcanic extrusives, but slower cooling generally favors exsolution. The spatial scale and degree of unmixing are variable and at least two mechanisms may be involved (e.g., Harrison & Putnis, 1999b). Spinodal decomposition initially produces small variations in chemical composition, with a wavelength on the order of 10 nm, and the amplitude of the variations increases as the process continues, resulting in a range of compositions while maintaining the cubic structure. Nucleation and growth begins with the formation of discrete regions having an equilibrium (solvus) composition (more Ti-rich or Ti-poor than the bulk composition) at the ambient temperature, and subsequently proceeds through growth of these nuclei by diffusion. In contrast, oxidation commonly causes another form of unmixing, oxyexsolution, forming lamellae of a Ti-rich rhombohedral phase (the endmember being ilmenite) within the Ti-depleted cubic host (Haggerty, 1991).

In our recent work on intermediate titanomagnetites ($0.25 < x < 0.4$) in young, rapidly cooled andesitic/dacitic ignimbrites from Mt. St. Helens and Novarupta (Bowles et al., 2013, 2015; Jackson & Bowles, 2014), we have documented large and reversible changes in TM Curie temperature ($\Delta T_c = 100°$ or more) that are produced by (a) protracted annealing at moderate temperature (300° to 400°C), which increases T_c, or (b) brief exposure to temperatures exceeding about 500° followed by rapid cooling, which decreases T_c. The exact mechanism underlying these large changes in T_c remains unclear, but the reversibility indicates that there is no bulk chemical alteration involved. Homogeneous oxidation during annealing could account for increases in T_c, but the subsequent decrease in T_c on rapid cooling from above 500°C cannot be due to chemical reduction. Thermomagnetic susceptibility $k(T)$ and $M_s(T)$ curves after annealing generally show single-phase behavior with no indication of unmixing. The changes in T_c are not accompanied by corresponding changes in M_s, and this fact appears to rule out significant intersite exchange of ferrous and ferric ions as the cause (supporting information in Bowles et al., 2013). This has more recently been confirmed in cation-distribution determinations (Lappe et al., 2015; Jackson et al., 2016) using X-ray circular magnetic dichroism (XMCD) and Mössbauer spectroscopy.

To help understand the nature of these fundamental property changes, we extend the investigation in this paper over a broader range of titanomagnetite compositions, ages, and origins. The expanded range of compositions will allow us to observe systematic relationships between ΔT_c, annealing T, and $T_{solvus}(x)$ and to evaluate the importance of effects like coupling of cation ordering and magnetic ordering (Burton, 1991; Harrison & Putnis, 1999b).

Table 1
Sample Properties

Sample ID	Lithology	Age/ date	Occurrence	Provenance	Reference	Mean $T_{c\text{-cooling}}$ [a]	Estimated x_{USP} [b]
10BT33H	Basalt	Miocene	Dike	Columbia River Basalt	Kelso et al. (2002)	367	0.47
FF02B	Rhyolitic Tuff	760 ka	Welded tuff	Bishop Tuff, Owens River Gorge, California	Gee et al. (2010)	548	0.05
FG1995–2	Basalt	1995	Flow	Fogo Volcano, Cape Verde	Brown et al. (2010)	179	0.58
KM039A	Andesitic- Dacitic Pumice	1912	Pyroclastic flow	Novarupta Volcano, Katmai, Alaska	Bowles et al. (2013)	355	0.35
LV17A	Andesite	1993	Lithic clast in pyroclastic deposits	Lascar Volcano, Chile	Paterson et al. (2010) and Paterson et al. (2010)	382	0.31
MSH02	Dacitic Pumice	1980	Pyroclastic flow	Mt. St. Helens Volcano, Washington State	Bowles et al. (2013)	341	0.37
SH14–2	Andesitic Pumice	2009	Pyroclastic flow	Soufrière Hills Volcano, Montserrat	Wadge et al. (2014)	394	0.29
SH-DC-3	Troctolite	1.1 Ga	Basal cumulate layered sequence	Duluth Complex	Wirth et al. (2011)	153	0.62
SK06	Gabbro		Sill	Northern Iceland	Horst (2013)	311	0.41
SK11	Gabbro		Sill	Northern Iceland	Horst (2013)	207	0.55
SK19	Gabbro		Sill	Northern Iceland	Horst (2013)	347	0.36
TC05–9	Rhyolitic Tuff		Welded tuff	Yucca Mountain, Nevada	Rosenbaum (1993)	518	0.1

[a]Curie temperatures from this study. [b]Calculated from T_c using the relation in Hunt et al. (1995); values calculated using the relations in Lattard et al. (2006) differ by only a few percent.

2. Materials and Methods

A new set of samples was collected from the Soufrière Hills volcano, Montserrat, in January 2014, for which the major results will be presented elsewhere; in this paper we focus on a single representative pumice sample. Additional new samples (Table 1), generously provided by various colleagues, include feeder dikes of the Columbia River basalts (provided by Basil Tikoff, UW-Madison, and Paul Kelso, Lake Superior State), a troctolite from the Duluth Complex (Sarah Brownlee, Wayne State), gabbro sills from northern Iceland (Andrew Horst, Oberlin), a basaltic lava from Fogo, Cape Verde (Maxwell Brown, University of Iceland), and pyroclastics and lavas from Lascar, Chile (Greig Paterson, Chinese Academy of Sciences, Beijing). These samples were solicited by us because of evidence that they exhibit the same sort of thermomagnetic irreversibility that we are investigating. Thus, we make no claim that they are generally representative of all natural titanomagnetites; nevertheless, they will allow us to show clearly that the phenomenon is not narrowly restricted to volcanic TM in young andesitic/dacitic pumices and ashes.

Previously studied pyroclastic samples from Mt. St. Helens and Novarupta were remarkably stable against chemical alteration during moderate-temperature (300–450°C) annealing in air for periods up to 10^3 h, and during thermomagnetic runs up to 600°C in air, which involved durations of <2 h at elevated temperature. During numerous heating-cooling cycles, the effects of oxyexsolution became gradually apparent by the increased proportion of susceptibility associated with $T_c > 500$°C (Bowles et al., 2013; Jackson & Bowles, 2014). In contrast, most of the new intrusive samples were found in preliminary runs to alter rapidly during heating in air, with the heating segment showing a homogeneous TM Curie temperature, generally less than 400°C, but the cooling segment additionally exhibiting something resembling an end-member magnetite T_c. For that reason, all specimens used in this study were prepared for a sequence of treatments and measurements in an inert atmosphere, by placing them in quartz tubes, repeatedly evacuating to less than 20 millitorr and flushing with pure nitrogen, and finally backfilling with nitrogen to a pressure of about 300 torr (roughly a third of a standard atmosphere) and sealing them shut. Fresh samples of Mt. St. Helens and Novarupta pumice were also included, to see whether their behavior in an inert atmosphere would differ from that previously observed in air. One Mt. St. Helens sample was mixed with graphite to produce a reducing environment during heating. These sealed specimens were subjected to a series of annealing treatments at temperatures from 325° to 425°C, for times ranging up to approximately 3,500 h, with various magnetic characterization experiments after each treatment.

The sealed tubes were of dimensions suitable for measurement in a Kappabridge KLY-2 furnace for $k(T)$ runs above room temperature, and in a Quantum Design MPMS for variable-frequency in-phase and out-of-phase $k(f,T)$ measurements below 300 K. Because the tubes were sealed, the conventional method of measuring temperature in the high-T experiments, by inserting a thermocouple, was not practicable. Therefore, temperatures were estimated according to the power supplied to the heater, using customized instrument control software. In a large number of calibration runs, we logged heater power and directly measured temperatures during heating and cooling, and the relationship was very reproducible. There is some uncertainty in absolute temperatures estimated from furnace power, due to factors including varying sample masses (thermal inertia) and imprecision in vertical placement of the tubes in the furnace. However, for measuring the Curie temperature difference between heating and cooling segments of an individual $k(T)$ run ($\Delta T_c = T_{c,heating} - T_{c,cooling}$), we found the power-calibrated estimates to provide very good accuracy. The use of sealed tubes also eliminated errors due to loss of material during transfer between containers for annealing and for thermomagnetic runs.

Isothermal annealing at five temperatures between 325 and 425°C was carried out in a horizontal tube furnace (Thermolyne 21100) for time intervals ranging from 1 hour to 3,450 h (144 days). Details are provided in the supporting information of this article. Samples that still exhibited significant thermomagnetic irreversibility after annealing at 425° received additional treatments at 450° and 475°C, to place an upper limit on the temperature range for the phenomenon in these samples. After each annealing treatment a high-T $k(T)$ data set was measured for each sample, using a heating/cooling rate of about 9°/min and normally with a maximum temperature of 650°C. During each $k(T)$ run approximately 11 min was spent within 50° of the maximum temperature for the run. In some cases the high-T run was preceded by a low-T ($<$300 K) $k(f,T)$ run. Church et al., (2011) have shown that such low-T measurements are sensitive probes of thermally activated electron hopping and magnetoelastic wall pinning in titanomagnetites. Overall, 36 annealing treatments were applied to each specimen, representing a cumulative time of about 2.5 years at elevated temperature.

A few additional samples were prepared for high-field hysteresis measurements at elevated temperature. These were mixed with a high-temperature epoxy (Omega CC) and sealed in repeatedly evacuated quartz tubes, in a final pure nitrogen atmosphere of 300 torr. They were then annealed, after which they were removed from their tubes for measurement on a vibrating sample magnetometer (Princeton MicroMag 3900) with a flow-through helium furnace. Measurements followed the saturation initial curve, $M_{si}(H,T)$, protocol of Fabian et al. (2013) to determine $M_s(T)$ and high-field slope $\chi_{hf}(T)$ at narrow temperature intervals through the magnetic order-disorder transition. As shown by Fabian et al. (2013), for ferrimagnetically ordered materials $\chi_{hf}(T)$ reaches a peak at or just above T_c. The mean-field modeling of Fabian et al. (2015) predicts a quantitative relationship between the area of the $\chi_{hf}(T)$ peak and the degree of chemical/cation ordering, specifically in the hematite-ilmenite solid solution; however, they noted that such peaks are a general feature of ferrimagnetically ordered materials. For our samples, we have done consecutive runs to observe the relation of $\chi_{hf}(T)$ to state of order. The first run, after annealing, has a relatively high degree of ordering and a correspondingly elevated T_c. Exposure to temperatures above T_c during the first run causes disordering, so after the relatively rapid cooling, the second run begins in a less ordered state with a correspondingly diminished T_c.

3. Measurement Results

3.1. High-Temperature Susceptibility

After annealing, most of the samples exhibit the same essential thermomagnetic irreversibility previously found in those from Mt. St. Helens and Novarupta: T_c is higher in the heating segment than in the cooling segment of the $k(T)$ runs (overview in Figures 1a and 1b, detailed presentation in supporting information Table S1 and figures). $T_{c,heating}$ increases systematically with annealing time t_a, and in most cases does not appear to reach a stable value even after 2,000+ hours. In contrast, $T_{c,cooling}$ is essentially independent of prior annealing history. Some of the samples contain multiple magnetic phases and have multiple corresponding Curie temperatures, seen most clearly in the derivative curves dk/dT (Figure 1b).

A near end-member magnetite component (T_c in the range 550–580°C) is visibly present in relatively small proportions in many of the samples (10BT33, FG1995–2, KM039, MSH002, SK06, SK19), and for

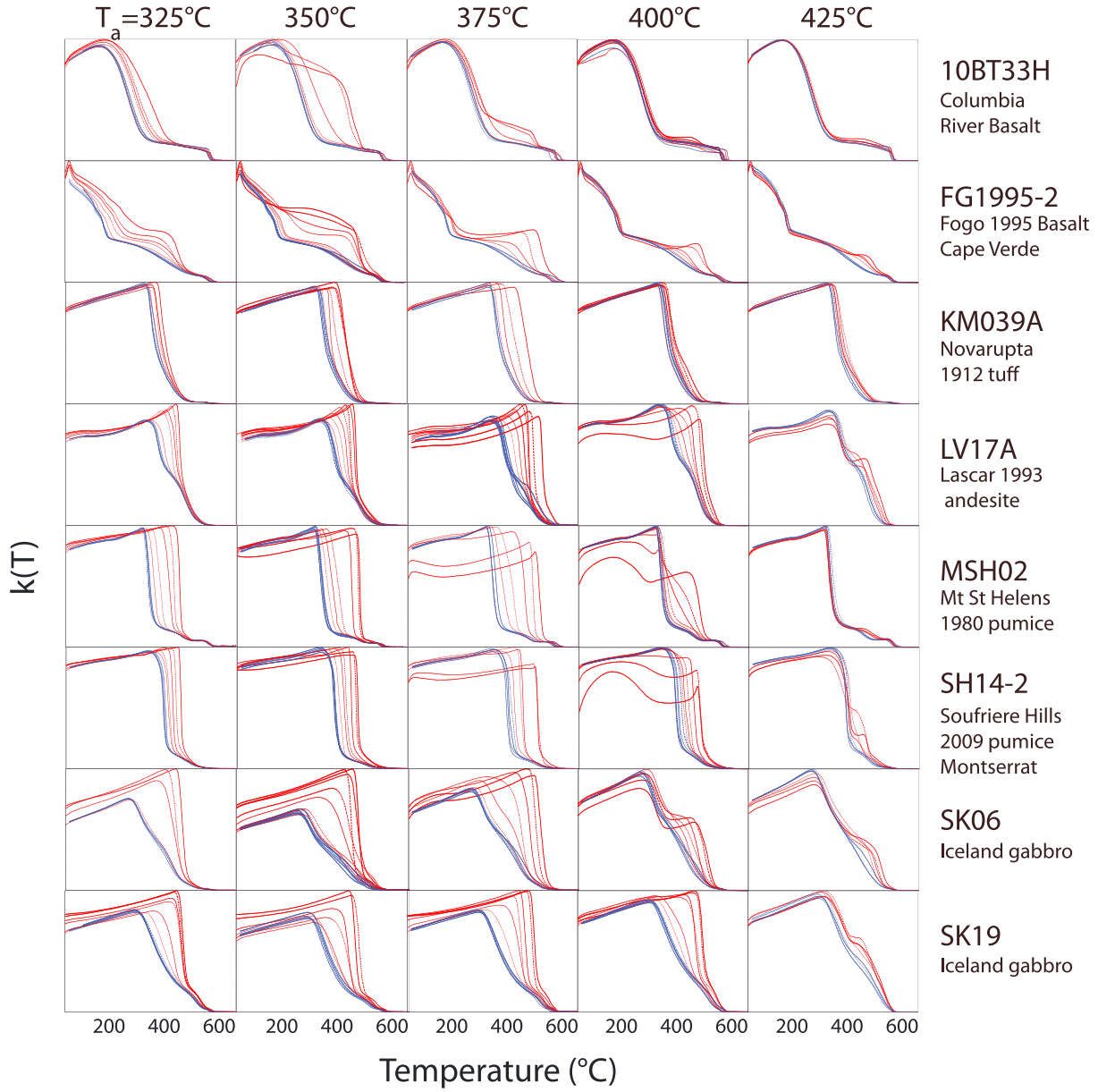

Figure 1a. Composite plots of thermomagnetic experiments on eight samples exhibiting similar essential behavior, with some significant variations. Red and blue curves respectively indicate heating and cooling segments of single-cycle $k(T)$ runs after different annealing times; annealing temperatures are given for each column. Heating segment Curie temperatures generally increase progressively with increasing annealing times at each temperature, whereas cooling segment curves are essentially independent of prior thermal history. More detailed plots are provided in the supporting information.

the most part the Curie temperature of this phase does not change significantly or systematically as a function of thermal history. This phase is clearly associated with oxyexsolved TM in the Novarupta and Mt. St. Helens samples (Bowles et al., 2013; Jackson & Bowles, 2014). Other detectable phases are presumably homogeneous titanomagnetites, and annealing clearly modifies their Curie temperature distributions. Most of the samples exhibit a well-defined dominant T_c in the heating and cooling segments, and for this phase $T_{c,cooling}$ ranges between about 180° (FG1995–2) and 400° (SH14–2), corresponding to nominal TM compositions in the range $0.58 > x > 0.29$, based on empirical calibrations (Hunt et al., 1995; Lattard et al., 2006). The Fogo sample is rather complex, with additional

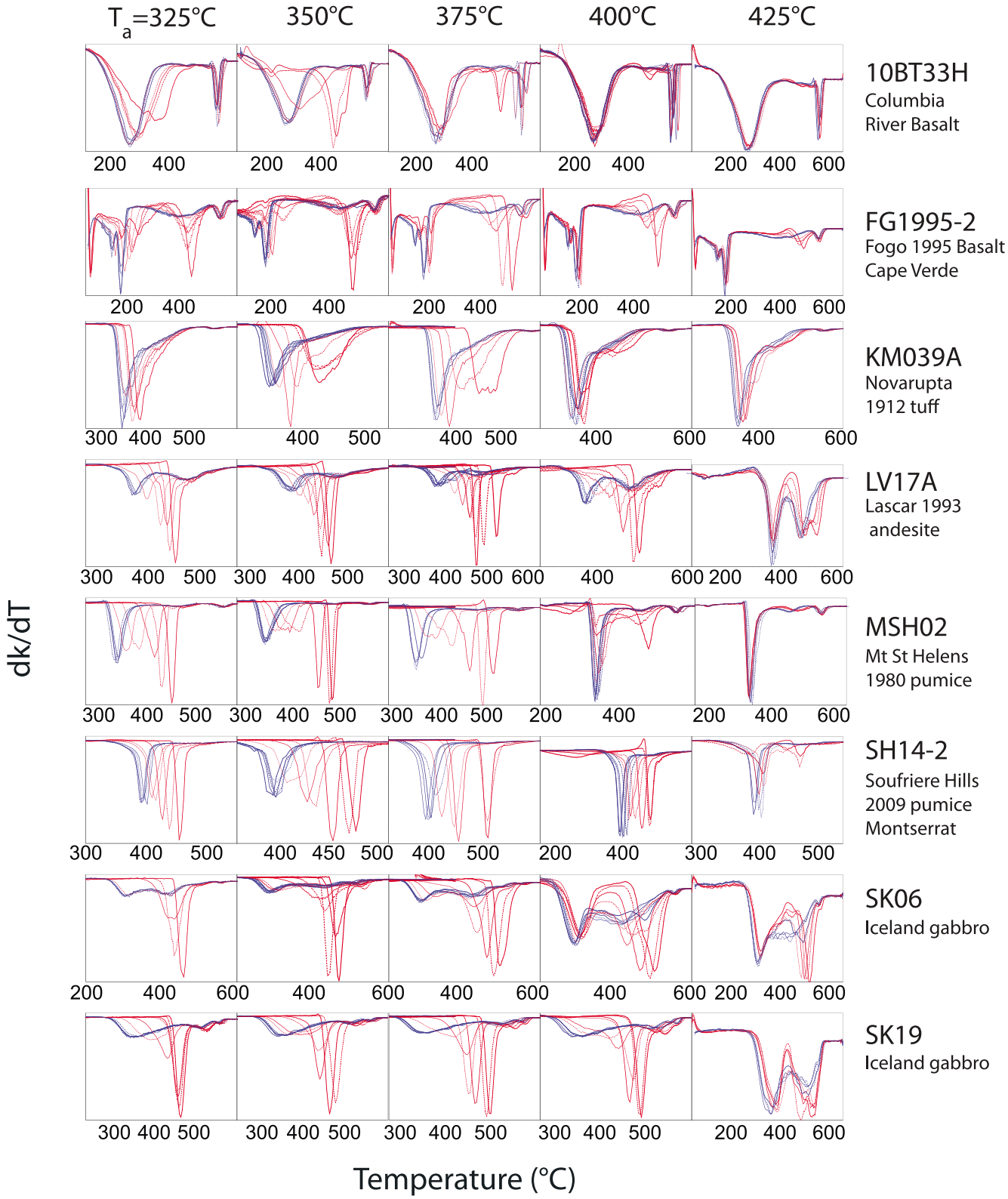

Figure 1b. Derivative curves for the single-cycle *k*(*T*) runs in Figure 1a; minima are used to quantify Curie temperatures. Note that horizontal scales are optimized to show detail and may not match those in Figure 1a.

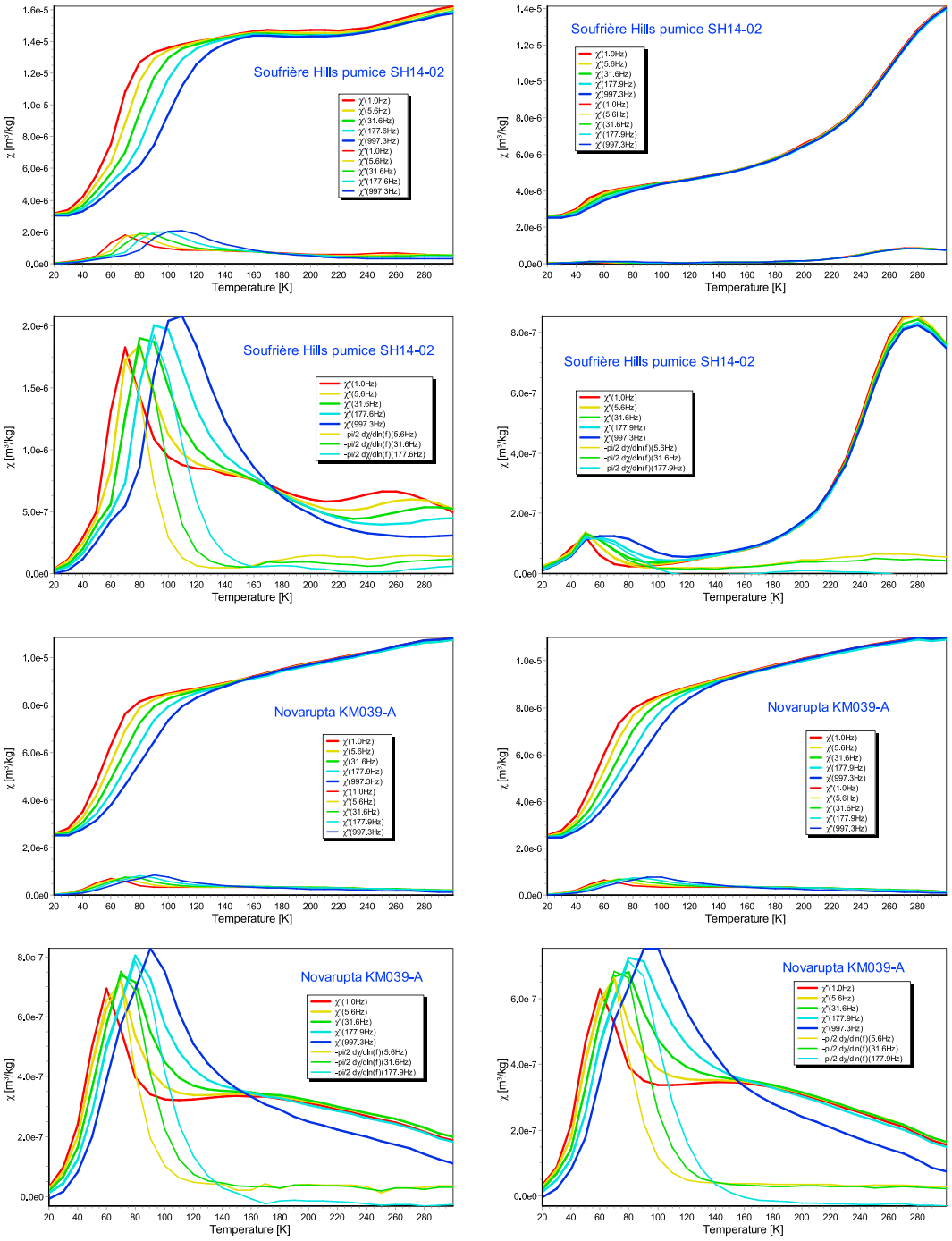

Figure 2. Low-temperature complex susceptibility for two samples: (left) after disordering by $k(T)$ run to 650°C; (right) after ordering by annealing at 375°C for 2,639 h. For each sample the upper plots show in-phase susceptibility χ' (bold curves) and quadrature susceptibility χ'' (fine) as functions of frequency (1 Hz (red) to 1000 Hz (blue)), and the lower plots show $\chi''(f, T)$ rescaled to show detail, compared with predicted values for a thermal relaxation mechanism.

well-defined Curie temperatures of 60° and 150°C ($x \sim 0.7$ and $x \sim 0.62$, respectively). The basaltic and gabbroic samples (10BT33 and the SK samples) have very broad minima in their cooling segment derivative curves, perhaps indicating a range of T_c due to compositional heterogeneity or spatially variable cation ordering.

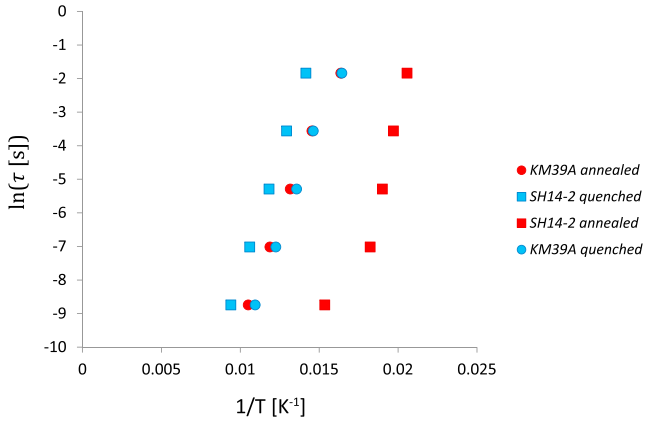

Figure 3. Arrhenius plot for the $k''(f,T)$ peaks in Figure 2.

For most of the samples, annealing at temperatures up to 350° or 375°C results in a homogeneous increase in T_c: after each annealing treatment a single major Curie temperature is found in the $k(T)$ heating curve, and T_c increases systematically as a function of annealing time. For higher annealing temperatures, there are more common indications of heterogeneous reordering: two major heating-curve Curie temperatures can be seen in each heating curve, and while the T_c values remain relatively constant, the susceptibility drop associated with each of them changes systematically with annealing time (e.g., 10BT33 at 375°C and above, FG1995–2 at all temperatures, and LV17A and SH14–2 at 425°C). Such heterogeneous ordering is well known in the magnesioferrite system and is thought to involve rapid nucleation of small regions of material with the equilibrium degree of order, followed by growth of these ordered regions at the expense of the remaining disordered material (Harrison & Putnis, 1999a).

In all cases the changes produced by annealing are rapidly erased in the highest-temperature part of the $k(T)$ run, so that the cooling curves are almost perfectly reproducible, independent of prior annealing treatments. For a few of the samples some minor cumulative alteration can be seen to have resulted from the repeated heatings (e.g., the Icelandic SK samples), and one sample (SK11) altered so significantly (supporting information) that it was removed from the experiment.

3.2. Low-Temperature Susceptibility

For many but not all of the samples, annealing also resulted in profound changes in $k(f, T)$ at low temperature; Figure 2 shows examples from Soufrière Hills, where annealing produced very large changes, and from Novarupta, where low-T changes due to annealing were insignificant, despite substantial changes in T_c. For both samples, in the low-T_c disordered state following a high-T thermomagnetic run, there is a sharp, step-like increase in the in-phase susceptibility $k'(f, T)$ at temperatures below about 140 K, accompanied by a very strong frequency dependence and a relatively large out-of-phase component (Figure 2, left). These features are very similar to those seen in relatively low-Ti ($x \leq 0.4$) titanomagnetites in a number of previous studies (e.g., Carter-Stiglitz et al., 2006; Church et al., 2011; Engelmann et al., 2010; Moskowitz et al., 1998; Radhakrishnamurty & Likhite, 1993). The out-of-phase susceptibility $k''(f, T)$ curves are sharply peaked, and at temperatures below the peak they match very precisely the values predicted by the theoretical "$\pi/2$" law for thermally activated processes (Egli, 2009; Mullins & Tite, 1973; Néel, 1949; Shcherbakov & Fabian, 2005): $k'' = -\pi/2\ dk'/d(\ln(f))$. Above the peak, k'' declines sharply but does not vanish, greatly exceeding the expected value for thermal relaxation; here the out-of-phase susceptibility is related primarily to weak-field hysteresis rather than to thermoviscous behavior (Jackson et al., 1998).

In the high-T_c ordered state following annealing at 375°C for 2,639 h (Figure 2, right), the step increase below 140 K is dramatically suppressed for the Soufrière Hills sample, as are the corresponding frequency dependence and out-of-phase susceptibilities. The relaxation peak in k'' is still present but less than one tenth its magnitude in the disordered state. There is a strong k'' peak near 260 K due to weak-field hysteresis, almost independent of frequency and 50–100% larger than k'' at the same T in the disordered state. In contrast, the Novarupta sample annealed at 375°C for 1,149 h shows essentially no change in low-temperature $k(f,T)$, even though the annealing caused a ΔT_c of 64°. Samples from Mt. St. Helens, Lascar, CRB, and Iceland all exhibited marked changes in $k(f,T)$ related to annealing, whereas samples from Novarupta and Fogo showed only subtle changes, despite the large changes in T_c visible in Figures 1a and 1b.

The activation energy E_a and time constant ("attempt time") τ_0 associated with the relaxation peak can be computed by fitting the $k''(f, T)$ data with an Arrhenius equation of the form $\tau = \tau_0 \exp(E_a/k_B T)$, where k_B is Boltzmann's constant and $\tau = 1/(2\pi f)$ is the measurement timescale. For each frequency (and its associated τ), the temperature at which the peak value of k'' occurs can be estimated by interpolating the location where the derivative $dk''/dT = 0$. The set of $k''(f, T)$ peaks thus yields a set of (τ, T) pairs which, when plotted on the Arrhenius diagram of $\ln(\tau)$ versus $1/T$ (Figure 3), define a line with slope E_a/k_B and intercept $\ln(\tau_0)$. Computed values are listed in Table 2.

Table 2
Relaxation Characteristics

	r^2	E_a (eV)	τ_0 (s)
S14–2 quenched	0.9998	0.13	1.75E-10
S14–2 annealed	0.8898	0.11	1.98E-13
(alternative calculation)	(0.9954)	(0.13)	(2.12e-15)
KM39A-quenched	0.9932	0.11	1.37E-10
KM39A-annealed	0.9950	0.10	6.41E-10

Annealing of SH14–2 not only diminishes the magnitude of the k'' peaks but also significantly decreases the temperatures at which they occur (range 71–106 K quenched versus 49–65 K after annealing); this is reflected in the shift of those points toward the right on the Arrhenius plot. The peaks are not very well defined in that data set, and the linearity in Figure 3 is correspondingly marginal, so the calculated parameters have relatively large uncertainty. On average the slope (E_a) is about the same as those for the other three data sets, and the intercept (attempt time) is significantly lower. An alternative approach to defining (τ, T) pairs for the Arrhenius fitting is to use the in-phase $k'(f, T)$ data, by determining either the temperature at which dk'/dT has a maximum for each frequency (e.g., Carter-Stiglitz et al., 2006), or the temperature at which k' reaches the approximate midpoint between pretransition and posttransition values for each frequency (e.g., Church et al., 2011; Özdemir et al., 2009). For the annealed SH14 sample, this yields better linearity ($r^2 = 0.9954$) and similar E_a (0.13 eV), but a significantly lower τ_0 (10^{-14} to 10^{-16}, depending on where the midpoint is chosen).

3.3. High-Temperature High-Field Measurements

The temperature dependence of saturation magnetization is very well defined by the $M_{si}(H,T)$ curves and, as predicted by Fabian et al. (2013, 2015), there is also a very clear peak in $\chi_{hf}(T)$ at or just above T_c (Figure 4). For the examples shown, T_c for the first run exceeds that for the second run by large amounts, with ΔT_c ranging from 41 to 84°, due to the increased order produced by annealing and the return to a more disordered state produced by exposure to higher temperatures during the first run. The relative $\chi_{hf}(T)$ peak areas are systematically related to T_c and thus to degree of order: peaks are largest for the most disordered states with the lowest Curie temperatures, and they become progressively smaller with increasing T_c and increasing order (Figure 4). After subtraction of a paramagnetic background trend (approximated as linear over this temperature interval), the calculated peak-area ratios A_2/A_1 (second run to first run) are respectively 1.5, 2.9, and 3.9 for Mt. St. Helens (MSH) samples 8J, 8M, and 2K (Figure 4).

3.4. Effects of Annealing Atmosphere

In our initial experiments (Bowles et al., 2013; Jackson & Bowles, 2014), the Mt. St. Helens and Novarupta samples were all annealed in air and showed essentially identical results for thermomagnetic runs in air and in inert Ar or He atmospheres, suggesting that the observed changes in T_c were not related to changes in sample stoichiometry. Nevertheless, stoichiometry is shown in our new experimental results to be an important factor.

Some samples that exhibited large ΔT_c after annealing in air showed much smaller changes after annealing in nitrogen. The Duluth Complex sample (SH-DC-2, Figure 5) and the Novarupta samples were quite sensitive to this change in annealing atmosphere. The Novarupta samples yielded ΔT_c values after annealing in N_2 about half as large as those for air anneals at corresponding T_a and t_a. Two companion specimens of the Duluth sample were measured prior to any laboratory annealing, one in air and one in low-pressure N_2, in a multicycle $k(T)$ run (Figure 5, top), which showed two magnetic phases: a near end-member magnetite (invariant T_c near 570°C) and a titanomagnetite whose T_c changes during the experiment. In each case the heating-cooling cycles are more or less reversible until peak temperatures reach about 500°C, after which each successive heating cycle to higher temperatures results in an incremental decrease in T_c for the titanomagnetite phase. This decrease is larger for the sample in N_2 than for that in air, which we attribute to partial oxidation of the TM in the latter sample during the heating-cooling cycles. Initial compositional differences are possible but less likely, as the two specimens were splits of the same crushed sample. Annealing of SH-DC-2 in air progressively increased the TM Curie temperature again, to around 400°C, and in the cooling curves, this was shifted back to below 300°. For the companion specimen sealed in N_2, the changes produced by annealing are much more subtle, consisting of only a slight shift toward higher T_c (Figure 5). Further, the significant difference persists in the cooling segment T_c of the TM (~150°C) with respect to that of the specimen annealed in air (~280°C; Figure 5), again suggesting a much greater cation deficiency in the air-annealed specimen.

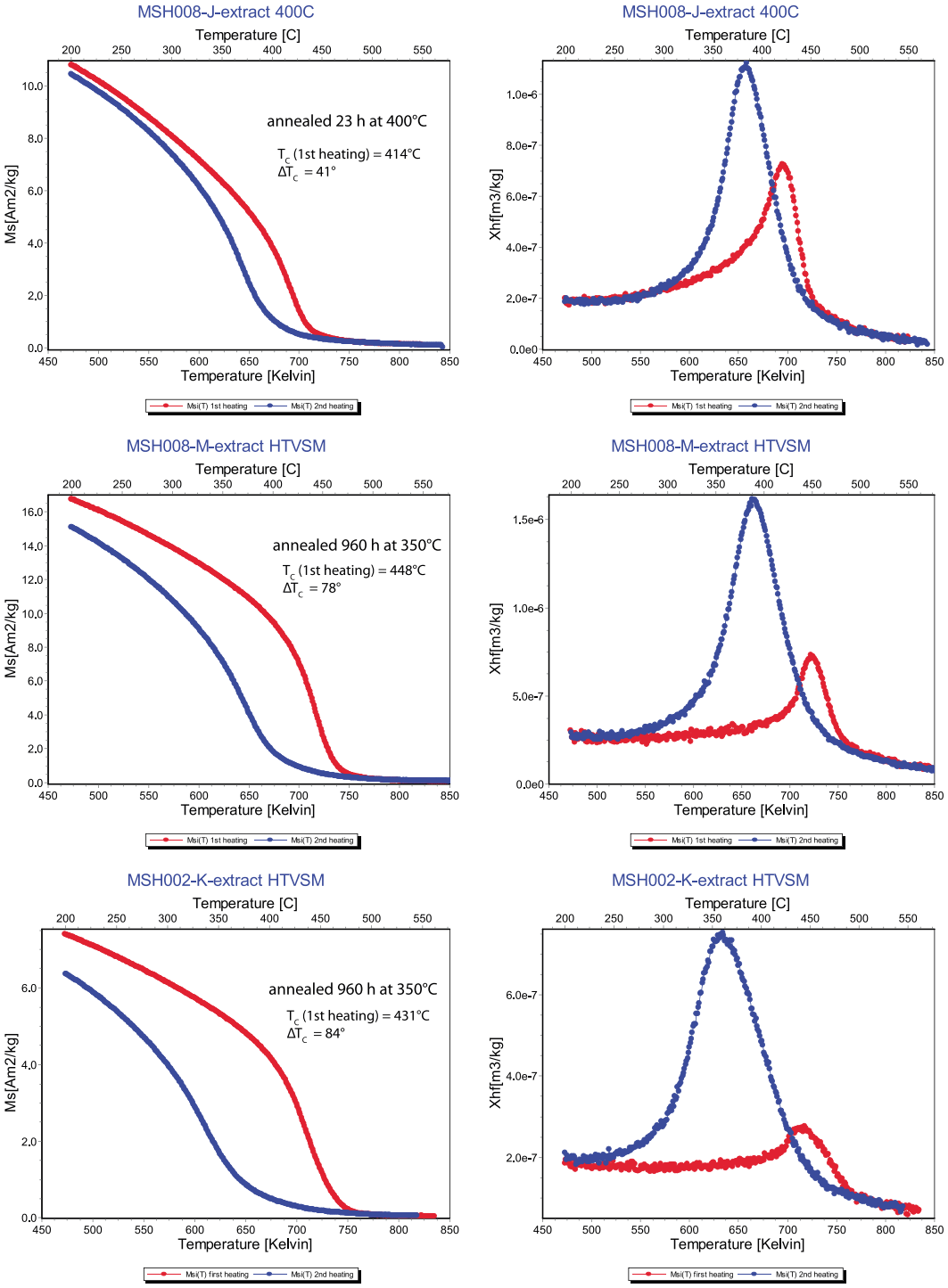

Figure 4. $M_s(T)$ (left) and $\chi_{hf}(T)$ (right) determined From $M_{si}(H,T)$ measurements at spacings of 5 mT and 1°C, for MSH specimens in different states produced by annealing. Red curves show values for the more ordered state during initial heating after annealing; blue curves show values for the more disordered state after cooling following the first run. Curie temperatures, significantly higher in the ordered state, are clearly recognizable by the sharp downward slope in $M_s(T)$ and by the peak in $\chi_{hf}(T)$, which is much larger in the disordered state.

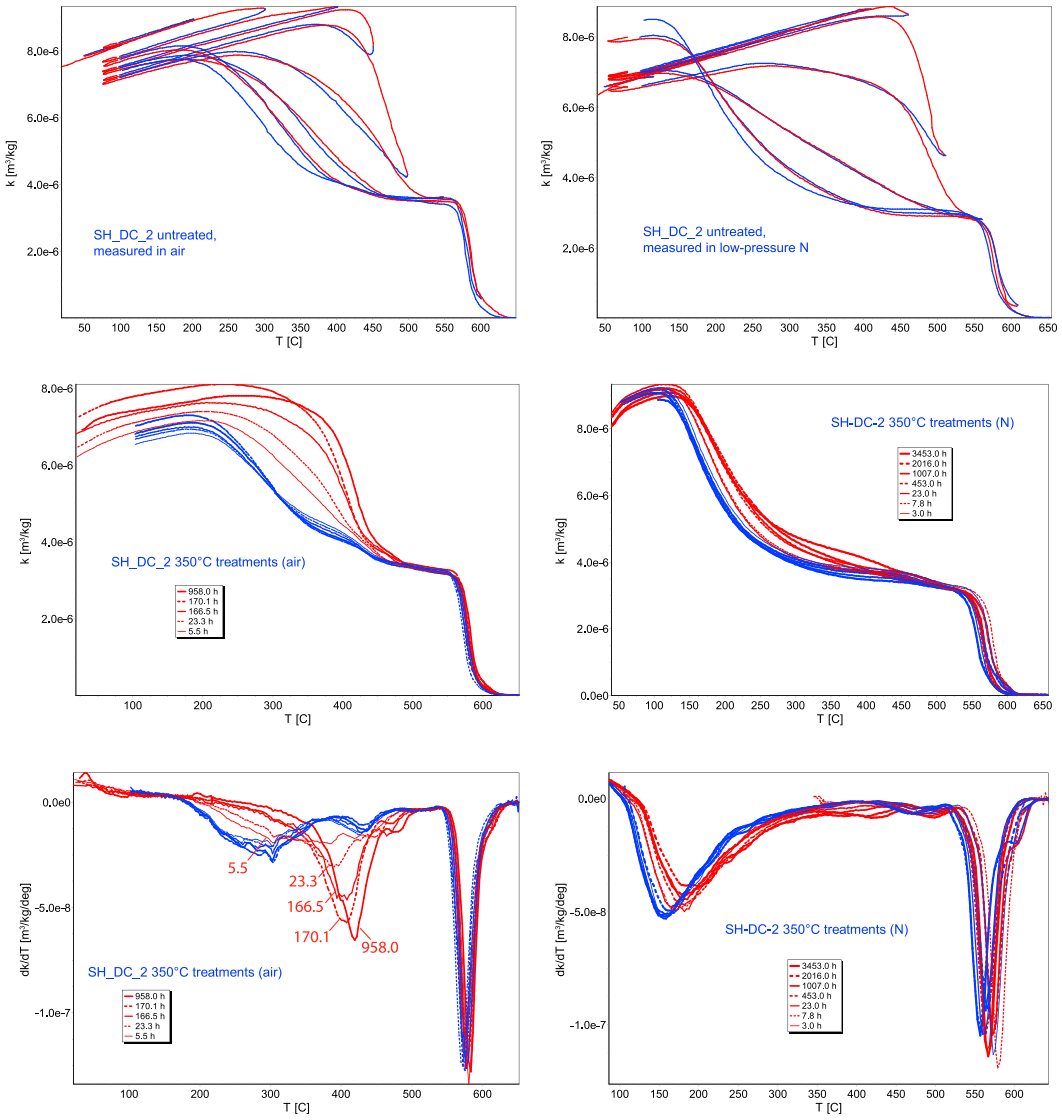

Figure 5. $k(T)$ for companion specimens of the Duluth complex troctolite, annealed and measured in air (left) and in inert nitrogen (right). Stepwise multicycle heating/cooling runs to increasingly higher temperatures for untreated samples (top) show a gradual decrease in T_c at temperatures above 450°C. Composite plots of single-cycle runs after annealing at 350°C for varying durations, showing $k(T)$ (middle) and dk/dT (bottom).

Both in air and in nitrogen the Mt. St. Helens samples showed very large changes in T_c, as in the previous studies, but in a reducing atmosphere (in the presence of graphite) the behavior gradually underwent a dramatic change (Figure 6). The first two heat treatments produced mostly homogeneous increases to very large values of ΔT_c, around 150° for $t_a > 1{,}000$ h, comparable to previous results, with some indication of heterogeneity after the second treatment (3,453 h). The third anneal (453 h) resulted in a distinctly heterogeneous reordering, with some portion of the TM retaining the lower T_c characteristic of the disordered state. After that, further anneals produced relatively small changes in Curie temperature ($\Delta T_c < 50°$) for most of the titanomagnetite in the sample, along with larger changes restricted to a very small fraction of the total TM volume. These results appear to indicate that some form of vacancy-mediated cation reordering occurs, even in a reducing atmosphere, during the 1,007 h anneal and again during the subsequent 3,453 h anneal, but eventually the vacancies are eliminated. Once that happens, annealing is no longer able to change the cation arrangements, and for all following treatments at any temperature, $\Delta\ T_c$ is insignificant.

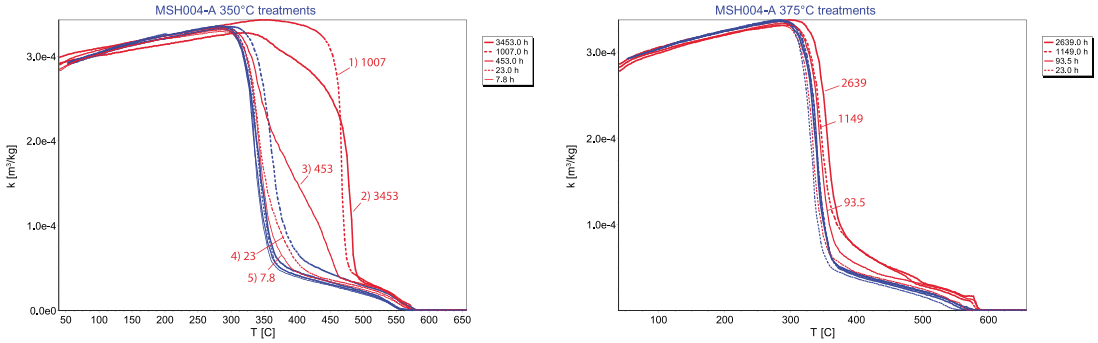

Figure 6. $k(T)$ for a magnetic extract of Mt. St. Helens ash mixed with graphite, sealed in an inert N_2 atmosphere, and annealed for varying durations, first at 350°C (left) and then at 375°C (right). The first anneal (1,007 h at 350°C) resulted in a large homogeneous increase in $T_{c\text{-heating}}$, and the second (3,453 h) resulted in a somewhat heterogeneous increase in $T_{c\text{-heating}}$ and a decrease in $T_{c\text{-cooling}}$ which persists for all subsequent cycles. After the third treatment (463 h) no further significant T_c increases were produced by annealing at any temperature.

4. Discussion of Results

4.1. Relation of Tc and Cation Ordering to Solvus and Magnetic Ordering

Previous investigations have linked titanomagnetite Curie temperatures to the ferrous-ferric site occupancy distribution (Bowles et al., 2013; Creer & Stephenson, 1972; Lattard et al., 2006; Stephenson, 1972b). In simple spinels containing two cation species, $A^{2+}B^{3+}{}_2O_4$, the "normal" arrangement is $A^{2+}[2B^{3+}]O_4$ (i.e., the divalent A cations are in the tetrahedral A sites and the trivalent B cations in the octahedral B sites, as in the mineral spinel) and the "inverse" arrangement is $B^{3+}[A^{2+}B^{3+}]O_4$ as in magnetite. In general, intersite cation ordering in simple two-cation spinels can be described by a distribution or inversion parameter b ($0 \le b \le 1$): $A^{2+}{}_{1\text{-}b}\ B^{3+}{}_b\ [A^{2+}{}_b\ B^{3+}{}_{2\text{-}b}]\ O_4$. In addition to Curie temperatures, the spontaneous magnetic moment per formula unit also varies with b: $m = m_A(2b - 1) + m_B(2 - 2b)$, where m_A and m_B are the individual cation moments. An alternative quantification is the order parameter $Q = 1 - 3b/2$, convenient for thermodynamic modeling and defined such that Q ranges from -0.5 for inverse ordering ($b = 1$), to 0 for random cation distribution ($b = ⅔$), to 1 for normal ordering ($b = 0$) (e.g., Harrison & Putnis, 1999b). In magnesioferrite (e.g., Harrison & Putnis, 1999a, 1999b), ordering is generally inverse ($-0.5 \le Q \le 0$), and the Curie temperature is a linear function of Q (and of b), with a maximum value in the fully inverse ordered state. For titanomagnetites, two distribution parameters and one composition parameter are required to specify the cation site occupancy (e.g., O'Neill & Navrotsky, 1984), and an order parameter would involve all of these. Stephenson's (1972b) model for titanomagnetites is formulated instead in terms of four cation site-occupancy parameters, and it, too, predicts a higher Curie temperature for more ordered arrangements: for intermediate compositions T_c is about 30° higher for the strongly (inverse) ordered cation distribution of Néel (1955) than for the more disordered distribution of Akimoto (1954). This difference, however, is much smaller than those that we observe. The modeling of Creer and Stephenson (1972) included Mg^{2+}, Al^{3+}, Mn^{2+}, and Cr^{3+} in proportions found in a set of natural titanomagnetites ($0.39 \le x \le 0.85$), using the Néel (1955) and Akimoto (1954) models as starting points, and inserting the other cations either randomly or in an ordered way according to estimated site preference energies. The range of calculated T_c values was fairly small for all samples (<30°), and surprisingly nonsystematic with respect to ordered/disordered distributions. For one sample, the most random arrangement (Akimoto model plus random insertion of other ions) had a T_c that exceeded that of the most ordered arrangement (Néel plus ordered insertion) by 13°.

Homogeneous intersite cation reordering is thought to occur in near-equilibrium conditions (i.e., when the degree of order at the ambient temperature $Q(T)$ is close to the equilibrium degree of order at that temperature $Q_{eq}(T)$) (Harrison & Putnis, 1999a). Heterogeneous ordering/disordering occurs in nonequilibrium conditions, when $Q(T)$ is significantly less/greater than $Q_{eq}(T)$. Although significant intersite ferrous/ferric cation reordering appears to be ruled out for our titanomagnetites by the invariance of low-T saturation magnetization and of Mössbauer and XMCD spectra (Fabian et al., 2015), the distinction between homogeneous and heterogeneous changes remains relevant in describing the shapes of the $k(T)$ curves and

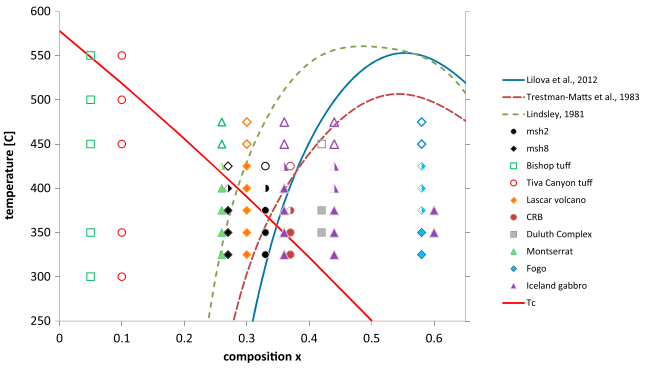

Figure 7. Summary of results of annealing/thermomagnetic experiments on various titanomagnetite-bearing intrusive and extrusive igneous rock units. Composition parameter x is the mole fraction of ulvöspinel, determined by electron microprobe for Mt. St. Helens (MSH) samples and estimated from cooling leg Curie temperatures for the other units. Solid symbols represent extended annealing experiments that resulted in a ΔT_c of at least 20°; half-filled symbols indicate significant heterogeneous changes in curie temperature; open symbols are for experiments that produced no significant change in the thermomagnetic characteristics. All data are for annealing treatments in low-pressure N_2 atmospheres except the bishop, Tiva canyon, and Duluth complex samples, which were annealed in air. The Novarupta samples overlap strongly with the Mt. St. Helens samples and are omitted for clarity. Solvus curves of Lindsley (1981), Trestman-Matts et al. (1983), and Lilova et al. (2012) shown for comparison; note that solid symbols generally occur near or below the solvus. Also shown for reference is the $T_c(x)$ curve of Lattard et al. (2006).

the corresponding distributions of T_c. It is reasonable to suppose that the observed changes in T_c are attributable to changes in short-range order of the intrasite cation distribution within the B sublattices. However, the process appears to differ in a fundamental way from that described by the thermodynamic model of Harrison and Putnis (1999b), since many of the largest ΔT_c values (implying a strongly nonequilibrium state at the start of annealing) are attained through homogeneous reordering (Figures 1a and 1b).

Our experimental results may be compared with two $T(x)$ functions to evaluate the importance of possible controls on ΔT_c due to annealing: the solvus temperature and the magnetic ordering temperature (Figure 7). For the latter, the reference curve $T_c = -150x^2 - 580x + 578$ (Bleil & Petersen, 1982; Lattard et al., 2006) is shown and is also used to calibrate the x coordinates of the data points, using the well-defined average value of $T_{c,cooling}$ for the major phase in each sample. Published binary solvus curves for pure TMs (without any additional substitute cations) are based on experimental data (e.g., Lindsley, 1981) or are calculated from thermodynamic models (Lilova et al., 2012; Trestman-Matts et al., 1983). The calculated solvus curves depend upon the cation distribution; Lilova et al. (2012) used XMCD and Mössbauer data to obtain a distribution very close to that of Kakol et al. (1991) and incorporated that into thermodynamic calculations to determine the solvus location.

Experimental results are summarized in Figure 7 with one data point for each sample at each annealing temperature, using filled symbols to indicate homogeneous changes with $\Delta T_c \geq 20°$, half-filled symbols for apparently heterogeneous changes with $\Delta T_c \geq 20°$, and open symbols for $\Delta T_c < 20°$. In several cases, for samples with multiple magnetic phases, there is some ambiguity in combining heating and cooling Curie temperatures to compute ΔT_c. For example, the Icelandic sample SK06 exhibits cooling segment derivative curves with two very broad minima at about 310° and 425°C (Figure 1b), which we assume to represent different TM compositions. Extended annealing at relatively low temperatures (up to 375°C) results in heating segment derivative curves having a single sharp minimum, at a temperature higher than either of the cooling segment minima, exceeding them respectively by approximately 200° and 75° (Figure 1b), each of which is a possible value for ΔT_c. For this reason we do not tabulate precise values of ΔT_c but summarize them in this semiquantitative way (Figure 7), and we plot the annealing results only at the x corresponding to the T_c of the major phase (310°C for SK06).

It is immediately apparent that significant changes in ΔT_c occur primarily under subsolvus conditions. However, the association is imperfect. If we take the most recent solvus of Lilova et al. (2012) as the most accurate, then many of the lower-x data with large ΔT_c actually plot above the solvus. On the other hand, the solvus calculations are for TMs free of Al, Mg, and other cations that occur in these natural titanomagnetites, and the effect of such additional substitution is to raise the solvus (e.g., Bowles et al., 2012), so it is probably safe to conclude that large increases in Curie temperature occur mainly or exclusively in subsolvus annealing conditions. This suggests an important role of chemical unmixing on some scale. However, it is also apparent that whereas the solvus temperature increases rapidly with increasing x in our region of interest, the upper limit of "effective" annealing temperatures (producing large ΔT_c) does not. For the whole range $0.25 < x < 0.6$, very large ΔT_c values generally occur for annealing temperatures up to about 400° and not above that (Figure 7). For the Ti-rich end of that range, this is well below the solvus, and one might expect chemical unmixing to proceed more rapidly at higher T, just below the solvus.

In the temperature range between about 425 and 525°C, the processes involved in decreasing T_c (cation disordering and/or chemical rehomogenization) begin to take rapid effect, and this appears to be the case for the full range of compositions in this study. Multicycle $k(T)$ runs commonly show the onset of irreversibility in this range (e.g., Figure 5, top; see also Bowles et al. (2013)). Figure 8 shows the maximum postannealing

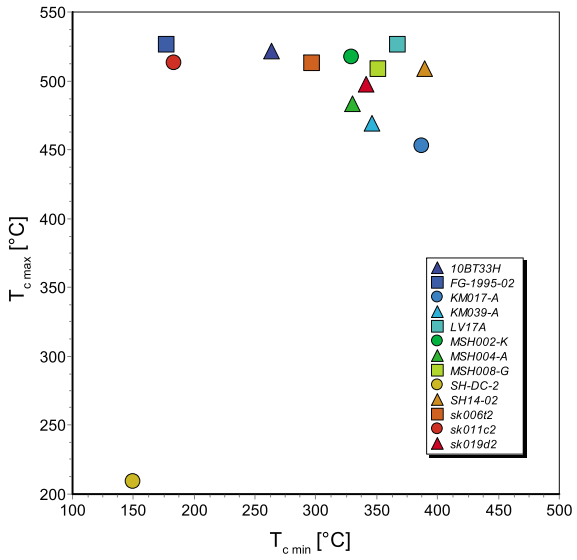

Figure 8. Minimum (quenched) and maximum (annealed) Curie temperatures for the samples sealed in inert atmospheres. We interpret T_c min as a proxy for TM composition by conventional calibration. Maximum Curie temperatures reached by annealing are generally in the 500°–525°C range, regardless of composition.

T_c (excluding that of any near-endmember magnetite) for each sample, plotted as a function of the corresponding quenched T_c, for all the samples annealed in low-pressure nitrogen atmospheres. Maximum Curie temperatures reached by annealing are generally in the 500°–525°C range, regardless of composition. Exceptions with lower $T_{c\ max}$ (the KM samples, MSH004 and SH-DC-2) all reached Curie temperatures in the 500°–525°C range when annealed in air. Thus, at this upper boundary, magnetic disordering coincides with chemical and/or cation disordering, and this explains why the $k(T)$ heating segment derivative curves (Figure 1b) become so sharp with increasing T_c. Harrison and Putnis (1999a, 1999b) have argued on both theoretical and experimental grounds that magnetic ordering and cation ordering are strongly coupled in both magnetite and magnesioferrite, and potentially in titanomagnetites as well.

4.2. Low-*T* Relaxation and Pinning Phenomena

For quenched samples, the step-like increase in low-*T* susceptibilities at about 50–100 K strongly resembles those previously documented in synthetic TMs with $x \leq 0.4$ (Carter-Stiglitz et al., 2006; Church et al., 2011; Engelmann et al., 2010; Moskowitz et al., 1998). These susceptibility steps were associated with isotropic points by Moskowitz et al. (1998), but Church et al. (2011) pointed out that for some compositions, the isotropic point is significantly higher than the susceptibility-step temperature. For the latter they proposed an intrinsic pinning transition, involving enhanced low-*T* anisotropy within domain walls, produced by a rearrangement of Fe^{2+} and Fe^{3+}ions inside the walls, enhancing the tetragonal magnetoelastic distortion associated with tetrahedral-octahedral ferrous-ion interactions. This hard intrinsic wall pinning also produces very high coercivities and distinctive FORC signatures at low temperatures (Church et al., 2011). The onset of thermally activated electron hopping on warming through the pinning transition relieves the distortion associated with the ferrous ions, decreasing the local anisotropy and wall pinning strength, and resulting in increased susceptibility and diminished coercivity.

When the same samples are run after annealing, the $k(f, T)$ curves often look very different, resembling those found for higher-Ti compositions ($x \geq 0.5$) (Moskowitz et al., 1998). Instead of a step, there is a gradual increase over the whole temperature range, with greatly diminished frequency dependence and out-of-phase components. Annealing thus has a very strong effect on the pinning transition and, by inference, on the short-range ordering of ferrous and ferric ions. These changes in low-*T* $k(T)$ behavior, like those in high-*T* behavior, are reversible: a sample can be repeatedly disordered by quenching from 600°C, which decreases its Curie temperature and restores the steplike low-*T* pinning transition, and then annealed, which increases T_c and broadens or suppresses the pinning transition.

The hard intrinsic pinning at low temperature may be considered as distinct from but related to disaccommodation, by which thermally activated diffusion of electrons, vacancies, or cations arranges them in a way that lowers the energy of domain walls and raises the energy required to displace the walls, thus stabilizing or pinning them (Moskowitz, 1985). Conventional disaccommodation experiments involve measurement of ac susceptibility at different times following alternating-field demagnetization (e.g.,Walz et al., 2003, 2007). The demagnetization leaves walls positioned quasi-randomly in local energy-minimum locations, and k is observed to decrease with time as the local minima are deepened, for example, by diffusion of vacancies or other defects into the walls. Such measurements as a function of temperature produce the disaccommodation spectrum, or relaxation spectrum. In general in ferrites, low-temperature disaccommodation on laboratory timescales involves diffusion of electrons; room-*T* disaccommodation is dominated by vacancy diffusion, and at higher temperatures cation diffusion becomes important (Moskowitz, 1985). Magnetite has disaccommodation peaks at about 30 K, 50–60 K, 120 K, and 300 K (Walz et al., 2003, 2007), temperatures where anomalies are also commonly found in susceptibility (Kosterov, 2003; Moskowitz et al., 1998; Özdemir et al., 2009) and in magnetic viscosity (Muxworthy & Williams, 2006). In synthetic titanomagnetites ($0 \leq x \leq 1$) Walz et al. (1997) found significant disaccommodation between 50 and 100 K for compositions TM10, TM20, and

TM30, but not for TM50 or more Ti-rich compositions; this corresponds closely to the temperature and the range of compositions where the susceptibility step transition is observed (Church et al., 2011; Moskowitz et al., 1998). Interestingly, in single-crystal titanomagnetites Walz et al. (2003, 2007) have documented a negative disaccommodation peak (indicating susceptibility increasing with time after AF demagnetization) at 65 K (close to the lowest-frequency k'' peak in our data), which they attribute to stress reduction due to the onset of electron hopping on warming. Church et al. (2011) interpret and model the phenomenon in terms of domain wall resonance in the temperature range where anisotropy related to electron hopping reaches a critical value.

Previous studies of the low-T susceptibility step transition in titanomagnetites have found a range of E_a and τ_0 values broadly similar to those in Table 2, and generally consistent with values expected for electron hopping (Walz et al., 2003, 2007; Walz & Kronmüller, 1994): Carter-Stiglitz et al. (2006) estimated an E_a of 0.1 eV for synthetic TM16 and TM35 but did not report a value for τ_0; Church et al. (2011) found an average activation energy of 0.13 ± 0.01 eV with an attempt time of 3.7×10^{-11} s, for compositions $x = 0.2$, 0.35, and 0.4. For pure magnetite, Muxworthy (1999) observed a similar step transition near 50 K and linked it with electron hopping, citing a change in τ_0 from 10^{-12} s above 50 K to 10^{-11} s below (Walz & Kronmüller, 1994). Similarly, Özdemir et al. (2009) found a significant frequency-dependent increase in susceptibility of pure magnetite near 30 K, but the values they calculated were rather different: $E_a = 0.035 \pm 0.005$ eV and $\tau_0 = 4.0 \times 10^{-9}$ s. They related this time constant to the atomic reorganization time between thermal excitations of small domain wall segments. The very short attempt times (10^{-13} to 10^{-16} s) calculated for our sample SH14–2 after annealing correspond to the range given by Walz et al. (2007) for the 65 K disaccommodation peak, but their calculated range of activation energy (0.18 to 0.23 eV) is significantly higher than our value for the postannealing k'' peak of SH14–2 (0.11 to 0.13 eV). Other samples that exhibit large changes in $k(f, T)$ after annealing (e.g., those from Mt. St. Helens) have postannealing relaxation peak activation energies ranging from 0.08 to 0.15 eV, and a very wide range of τ_0 values that are generally sensitive to the details of how they are determined, due to the log scaling of the vertical axis in the Arrhenius plot. Overall, it seems fairly clear that the step transition involves the onset of electron hopping on warming (Church et al., 2011) and that for many samples the process is strongly affected by prior annealing, but many of the details remain unclear. One may speculate in a general way that annealing increases the vacancy concentration, or ordering of vacancies and nonmagnetic cations, in such a way that ferrous-ferric electron hopping is suppressed.

A question that demands to be asked, but that is difficult to answer, is why some samples show changes in low-temperature behavior and others do not, when all of them exhibit significant changes in high-T behavior related to annealing history. The Novarupta and Soufrière Hills samples are nearly indistinguishable in their $k(f,T)$ results after rapid cooling from 650°C. After annealing their low-T $k(f,T)$ curves are dramatically different from each other (Figure 2), yet their high-T thermomagnetic curves are very similar. This suggests that there are no significant differences in their compositions or oxidation states, and perhaps that different mechanisms or different scales of order/disorder in the arrangement of cations and vacancies are responsible for changes in the Curie temperature and in the low-T pinning transition.

4.3. $\chi_{hf}(T)$ Peaks

The mean field modeling of ferrimagetic solid solutions by Fabian et al. (2015), using the exchange-link geometries and constants for homogeneous ferrian ilmenites, predicts a direct relationship between the area of the $\chi_{hf}(T)$ peak and the degree of chemical/cation ordering (order parameter Q). In the ferrian ilmenites, order ($0 \leq Q \leq 1$) is related to confinement of Ti^{4+} to alternating c planes, and increases in Q cause increases in M_s but do not significantly affect T_c. (Fabian et al., 2015). In our experiments there are, as predicted, clear peaks in $\chi_{hf}(T)$ at T_c, and a significant correlation between the peak areas and the degree of order inferred from T_c. Interestingly, however, the relationship for our TMs is an inverse one: the more ordered states with higher T_c exhibit much smaller $\chi_{hf}(T)$ peaks than the relatively disordered states with lower T_c. Clearly, there are significant differences between TM spinels and rhombohedral ferrian ilmenites, in crystal structure, cation ordering, and magnetic ordering, that may account for their different $\chi_{hf}(T)$ behavior. Ordering in the hematite-ilmenite series is convergent: the sublattices lose their crystallographic distinction when the cations are randomly distributed; whereas in spinels the tetrahedral and octahedral sites always remain distinct and cation ordering is nonconvergent. Detailed mean field modeling for variably substituted and cation-deficient

TM spinels is far beyond the scope of this paper, but the experimental results are very robust and support the inference that some form of chemical/cation reordering occurs in the annealing-quenching cycles, albeit a reordering that does not strongly affect M_s.

There has long been speculation that some form of chemical clustering or short-range order within the B sites may play a significant role in the magnetic properties of titanomagnetites, based on Mössbauer spectroscopy, neutron diffraction, and other data (e.g., Jensen & Shive, 1973; Moskowitz, 1987; Wechsler et al., 1984). Subsolidus B-site chemical clustering was also observed in the thermodynamic cation distribution models of Harrison et al. (2013) for the magnesioferrite-qandilite solid solution ($MgFe_2O_4$-Mg_2TiO_4, an analog of the titanomagnetites), on a scale of several unit cells. They suggested that such short-range clustering of octahedral cations is an intrinsic part of the cation ordering/disordering process for intermediate compositions in the vicinity of a solvus (Harrison et al., 2013). The length scale of this clustering is small enough for the material to behave homogeneously in terms of its magnetic ordering; it effectively acts as a nanocomposite material, with a single T_c higher than the volume average of the Curie temperatures of the segregated compositions (Skomski & Sellmyer, 2000).

4.4. Nonstoichiometry

The experiments with differing annealing atmospheres (Figures 5 and 6) make it clear that the largest changes in T_c occur in cation-deficient titanomagnetites. A distinction is conventionally made between homogeneous oxidation at elevated temperatures, which allows only low degrees of nonstoichiometry (e.g., Senderov et al., 1993), and heterogeneous oxidation at lower temperature, in which high degrees of overall nonstoichiometry can slowly develop, initially by surface oxidation and subsequently by diffusion along the oxidation gradient within the core-shell particle structure (e.g., O'Reilly, 1984; Özdemir & Dunlop, 2010; van Velzen & Dekkers, 1999). In our samples either or both of these processes may have been active in nature, and some amount of low-temperature oxidation may have occurred during laboratory annealing, even in the inert atmosphere.

Several previous studies on high-T (1000°C and above) synthesis and annealing have indicated a relationship between cation ordering and cation deficiency (controlled by oxygen fugacity) (e.g., Lattard et al., 2006; Wanamaker & Moskowitz, 1994). A large single crystal of TM60 synthesized by Wanamaker and Moskowitz (1994) had a small gradient in Ti concentration and a more significant gradient in vacancy concentration, as a consequence of the method of production. They documented significant differences (up to about 50°) in T_c across the crystal and demonstrated by high-T annealing (1300°C) in different fO_2 that these were due to differences in nonstoichiometry, with inferred accompanying differences in cation ordering (Wanamaker & Moskowitz, 1994). This is broadly consistent with our inference that cation deficiency enables the existence of high-T_c cation distributions.

Lattard et al. (2006) synthesized sets of titanomagnetites with $0 < x < 1$, and with fO_2 at the upper and lower limits of single-phase TM stability (i.e., a more oxidized set in equilibrium with hematite-ilmenite solid-solution phases and a more reduced set in equilibrium with wüstite), at temperatures of 1100° and 1300°C. Under these conditions the more oxidized sets are expected to have the highest possible vacancy concentrations, and the more reduced sets to be free of vacancies (Lattard et al., 2006; Senderov et al., 1993). They observed a thermomagnetic irreversibility in these samples similar to that in ours, but of smaller magnitude and in the opposite sense: $T_{c,heating} < T_{c,cooling}$. They attributed this to a relatively low degree of cation order quenched in following synthesis, and a correspondingly low T_c at the start of the thermomagnetic run. On heating above a relaxation temperature in the $k(T)$ experiment (less than that during rapid quenching), the cation distribution was postulated to re-equilibrate to a higher degree of order, which is preserved on cooling through the closure temperature, and hence, T_c is higher on cooling. The differences in T_c were much larger (up to 45°) for the samples with higher vacancy concentration (synthesized under higher fO_2) than for the stoichiometric samples, for which ΔT_c did not exceed 10°.

MSH samples commonly contain coexisting TM and titanohematites (TH, hematite-ilmenite solid-solution phases), indicating relatively oxidizing conditions of crystal growth, and resultant cation deficiency. The compositions of the cubic and rhombohedral oxide phases allow estimation of the (T, fO_2) conditions in which they were in equilibrium (Ghiorso & Evans, 2008; Lindsley, 1977; Sauerzapf et al., 2008). Melson and Hopson (1981) determined TM and TH compositions of the 1980 Mt. St. Helens erupted materials by

electron microprobe and found average compositions of TM30 (x = 0.3) and TH80 (y = 0.8 in $Fe_{2-y}Ti_yO_3$ ($0 \le y \le 1$)). Using the calibration of Lindsley (1977), they estimated pre-eruption temperatures near 1000°C and fO_2 about 1 log unit above the Ni-NiO buffer (Melson & Hopson, 1981). In low-T $k(f, T)$ measurements we see Néel points in some MSH sites in the range 150–270 K, corresponding to TH compositions in the range $0.85 \ge y \ge 0.78$ (Engelmann et al., 2010), and for all MSH sites $T_{c,cooling}$ is in the range 330° to 400°C, corresponding to pure TM compositions in the range $0.4 \ge x \ge 0.31$ (curve 1 of Lattard et al., 2006, equilibrated with ilmenite), both of which agree well with the results of Melson and Hopson (1981). Thus, the MSH samples, which remain the best examples of malleable TM Curie temperatures, may be inferred to have a significant vacancy concentration, which in turn may be inferred to play a key role in changing T_c by annealing and quenching. The inference is confirmed by the permanent loss of this transformability due to annealing in a reducing atmosphere.

5. Summary and Conclusions

Titanomagnetites with a range of compositions, ages, cation substitutions, and vacancy concentrations have Curie temperatures that are strongly sensitive to thermal history, both in nature and in the laboratory. Annealing at moderate temperatures (approximately 300° to 425°C) can cause significant increases in T_c, by 100° or more, and the increases can be reversed by brief exposure to temperatures exceeding 450° to 500°C. These changes are not due to homogeneous oxidation/reduction, exsolution/rehomogenization, or intersite cation ordering/disordering, but appear to arise from some nanoscale mechanism that is related to each of these (Bowles et al., 2013; Jackson & Bowles, 2014). Our new experimental results show that these changes in T_c occur over a wider range of compositions than previously documented, and that redox conditions and cation deficiency play significant roles. Repeatable T_c enhancement appears to be largely restricted to subsolvus conditions and inert or oxidizing atmospheres. However, the upper bound on annealing temperatures that produce large ΔT_c does not appear to follow the solvus closely and seems to be nearly independent of TM composition within the range $0.25 \le x \le 0.6$. Likewise, quenching from any temperature above about 500°C restores T_c to a repeatable base level for each sample, and this closure temperature is almost independent of composition within the range studied.

Accompanying the changes in Curie temperature are strong changes in low-temperature relaxation phenomena, seen in frequency-dependent complex susceptibility measurements. For samples in the quenched, low-T_c state, the activation energy and time constant associated with a set of out-of-phase susceptibility peaks between about 50 and 120 K are around 0.12 eV and 10^{-10}s, respectively, similar to those determined by Walz et al. (2007) for electron tunneling (0.03 eV and 10^{-10} s) and electron hopping (0.25 eV and 10^{-12} s) in magnetite, and for Ti^{4+}-modified electron hopping (0.18–0.23 eV and 10^{-13}–10^{-17} s) in TM20. In the annealed, high-T_c state, the out-of-phase peaks are strongly suppressed for most samples, and shifted to somewhat lower temperatures, yielding E_a and τ_0 of 0.11–0.13 eV and 10^{-13}–10^{-15} s. Electron hopping relieves some of the stress associated with Fe^{2+}, decreasing anisotropy and unpinning domain walls and increasing susceptibility (e.g., Church et al., 2011). In the annealed state this unpinning appears to occur gradually over the whole temperature range from 30 K to room T.

Hysteresis measurements at narrow temperature intervals across the magnetic order-disorder transition show that as saturation magnetization vanishes, high-field susceptibility reaches a maximum, as predicted by Fabian et al. (2015) for ferrimagnets in general and for ferrian ilmenites in particular. In the ferrian ilmenites, with increasing order parameter Q (increasing segregation of Ti into alternating c plane layers), T_c changes only minimally, whereas $M_s(0)$ and $\chi_{hf}(T_c)$ increase significantly. By contrast, in our TM samples, we suggest that annealing causes an increase in some short-range order parameter q, and that T_c increases in parallel, whereas $M_s(0)$ changes only minimally and $\chi_{hf}(T_c)$ decreases.

Acknowledgments

We are indebted to our colleagues who donated samples included in this study: Andrew Horst, Paul Kelso, Basil Tikoff, Samer Hariri, Sarah Brownlee, Maxwell Brown, and Greig Paterson. We thank Bruce Moskowitz for illuminating discussions and for helpful comments and suggestions on the manuscript. We also thank Nathan Church and Valera Shcherbakov for thoughtful reviews and Richard Harrison and Karl Fabian for discussion of many of the ideas in this paper. Credit is also due to Peat Sølheid, who provided essential help with sample preparation and instrument configuration. Basic data (annealing times and temperatures and resultant Curie temperatures measured while heating and cooling) are provided in the supporting information for this paper. More detailed data ($k(T)$ thermomagnetic curves, low-T complex susceptibility data, and high-T hysteresis data) will be made available through the Magnetics Information Consortium (MagIC) database (earthref.org/MAGIC/). The project has been supported by NSF Geophysics program grants EAR-1315845 (to M. J.) and 1315971 (to J. B.) and has benefitted by access to the facilities of the Institute for Rock Magnetism, funded by the NSF Instruments and Facilities program. This is IRM contribution 1703.

References

Akimoto, S. (1954). Thermo-magnetic study of ferromagnetic minerals contained in igneous rocks. *Journal of Geomagnetism and Geoelectricity*, *6*(1), 1–14. https://doi.org/10.5636/jgg.6.1

Bleil, U., & Petersen, N. (1982). Magnetic properties of natural minerals. In G. Angenheister (Ed.), *Landolt-Börnstein: Zahlenwerte und Funktionen aus Naturwissensschaft und Technik, Neue Serie V, Band 1b* (pp. 308–365). Heidelberg, New York: Springer-Verlag.

Bowles, J. A., Gee, J. S., Jackson, M., & Avery, M. (2015). Geomagnetic paleointensity in historical pyroclastic density currents: Testing the effects of emplacement temperature and postemplacement alteration. *Geochemistry, Geophysics, Geosystems*, *16*(10), 3607–3625. https://doi.org/10.1002/2015GC005910

Bowles, J. A., Jackson, M., Berquó, T. S., Sølheid, P. A., & Gee, J. S. (2013). Inferred time- and temperature-dependent cation ordering in natural titanomagnetites. *Nature Communications*, *4*, 1916. https://doi.org/10.1038/ncomms2938

Bowles, J. A., Tatsumi-Petrochilis, L., Hammer, J. E., & Brachfeld, S. A. (2012). Multi-component cubic oxide exsolution in synthetic basalts: Temperature dependence and implications for magnetic properties. *Journal of Geophysical Research*, *117*, B03202. https://doi.org/10.1029/2011JB008867

Brown, M. C., Feinberg, J. M., & Bowles, J. A. (2010). *Comparison of palaeointensity methods using historical lavas from Fogo, Cape Verde*, Abstract GP11A-0742. Paper Presented at AGU Fall Meeting, American Geophysical Union, San Francisco.

Burton, B. P. (1991). The interplay of chemical and magnetic ordering. *Reviews in Mineralogy*, *25*, 303–321.

Carter-Stiglitz, B. S., Moskowitz, B., Solheid, P., Berquó, T. S., Jackson, M., & Kosterov, A. (2006). Low-temperature magnetic behavior of multi-domain titanomagnetites: TM0, TM16, and TM35. *Journal of Geophysical Research*, *111*, B12S05. https://doi.org/10.1029/2006JB004561

Church, N., Feinberg, J., & Harrison, R. (2011). Low-temperature domain wall pinning in titanomagnetite: Quantitative modeling of multidomain first-order reversal curve diagrams and AC susceptibility. *Geochemistry, Geophysics, Geosystems*, *12*(7), Q07Z27. https://doi.org/10.1029/2011GC003538

Creer, K. M., & Stephenson, A. (1972). Some consequences of aluminum and magnesium impurities in naturally occurring titanomagnetites. *Journal of Geophysical Research*, *77*(20), 3698–3710. https://doi.org/10.1029/JB077i020p03698

Dunlop, D. J., & Özdemir, Ö. (1997). *Rock magnetism: Fundamentals and frontiers*, *Cambridge studies in magnetism* (Vol. 573). Cambridge: Cambridge University Press. https://doi.org/10.1017/CBO9780511612794

Egli, R. (2009). Magnetic susceptibility measurements as a function of temperature and frequency I: Inversion theory. *Geophysical Journal International*, *177*(2), 395–420. https://doi.org/10.1111/j.1365-246X.2009.04081.x

Engelmann, R., Kontny, A., & Lattard, D. (2010). Low-temperature magnetism of synthetic Fe-Ti oxide assemblages. *Journal of Geophysical Research*, *115*, B12107. https://doi.org/10.1029/2010JB000865

Evans, M. E., & Heller, F. (2003). *Environmental magnetism: Principles and applications of environmagnetics*. Amsterdam: V., Academic Press, Elsevier Science.

Fabian, K., Shcherbakov, V. P., & McEnroe, S. A. (2013). Measuring the Curie temperature. *Geochemistry, Geophysics, Geosystems*, *14*(4), 947–961. https://doi.org/10.1029/2012GC004440

Fabian, K., Shcherbakov, V. P., McEnroe, S. A., Robinson, P., & Burton, B. P. (2015). Magnetic mean-field modelling of solid solutions: Theoretical foundations and application to the hematite–ilmenite system. *Geophysical Journal International*, *202*(2), 1029–1040. https://doi.org/10.1093/gji/ggv199

Gee, J. S., Yu, Y., & Bowles, J. (2010). Paleointensity estimates from ignimbrites: An evaluation of the bishop tuff. *Geochemistry, Geophysics, Geosystems*, *11*(3), Q03010. https://doi.org/10.1029/2009GC002834

Ghiorso, M. S., & Evans, B. W. (2008). Thermodynamics of rhombohedral oxide solid solutions and a revision of the Fe-Ti two-oxide geothermometer and oxygen-barometer. *American Journal of Science*, *308*(9), 957–1039. https://doi.org/10.2475/09.2008.01

Haggerty, S. E. (1991). Oxide textures—A mini-Atlas. *Reviews in Mineralogy*, *25*, 137–220.

Harrison, R. J., Palin, E. J., & Perks, N. (2013). A computational model of cation ordering in the magnesioferrite-qandilite ($MgFe_2O_4$-Mg_2TiO_4) solid solution and its potential application to titanomagnetite (Fe_3O_4-Fe_2TiO_4). *American Mineralogist*, *98*(4), 698–708. https://doi.org/10.2138/am.2013.4318

Harrison, R. J., & Putnis, A. (1999a). Determination of the mechanism of cation ordering in magnesioferrite ($MgFe_2O_4$) from the time- and temperature-dependence of magnetic susceptibility. *Physics and Chemistry of Minerals*, *26*(4), 322–332. https://doi.org/10.1007/s002690050192

Harrison, R. J., & Putnis, A. (1999b). The magnetic properties and crystal chemistry of oxide spinel solid solutions. *Surveys in Geophysics*, *19*(6), 461–520. https://doi.org/10.1023/a:1006535023784

Hauptman, Z. (1974). High temperature oxidation, range of non-stoichiometry, and Curie point variation of cation deficient titanomagnetite $Fe_{2.4}Ti_{0.6}O_{4+\gamma}$. *Geophysical Journal of the Royal Astronomical Society*, *38*(1), 29–47. https://doi.org/10.1111/j.1365-246X.1974.tb04107.x

Horst, A. J. (2013). Structure and accretion at mid-ocean ridges with high magma supply: Perspectives from seafloor escarpments and Iceland (PhD thesis). Syracuse University.

Hunt, C. P., Moskowitz, B. M., & Banerjee, S. K. (1995). Magnetic properties of rocks and minerals. In T. J. Ahrens (Ed.), *A handbook of physical constants* (Vol. 3, pp. 189–204). Washington, DC: American Geophysical Union.

Jackson, M., & Bowles, J. A. (2014). Curie temperatures of titanomagnetite in ignimbrites: Effects of emplacement temperatures, cooling rates, exsolution, and cation ordering. *Geochemistry, Geophysics, Geosystems*, *15*(11), 4343–4368. https://doi.org/10.1002/2014GC005527

Jackson, M., Bowles, J. A., Lappe, S.-C. L. L., & Solheid, P. (2016). *Titanomagnetite curie temperatures: Effects of vacancies, chemical/cation ordering and thermal history*, Abstract GP31A-1284. Paper presented at AGU Fall Meeting, San Francisco, CA.

Jackson, M., Moskowitz, B., Rosenbaum, J., & Kissel, C. (1998). Field-dependence of AC susceptibility in titanomagnetites. *Earth and Planetary Science Letters*, *157*(3-4), 129–139. https://doi.org/10.1016/S0012-821X(98)00032-6

Jensen, S. D., & Shive, P. N. (1973). Cation distribution in sintered titanomagnetites. *Journal of Geophysical Research*, *78*(35), 8474–8480. https://doi.org/10.1029/JB078i035p08474

Kakol, Z., Sabol, J., & Honig, J. M. (1991). Cation distribution and magnetic properties of titanomagnetites $Fe_{3-x}Ti_xO_4 (0 \leq x < 1)$. *Physical Review B*, *43*(1), 649–654. https://doi.org/10.1103/PhysRevB.43.649

Kelso, P. R., Kelts, A. B., Giorgis, S., Tikoff, B., Klein, R. W., Szczepanek, B. P., … Theiner, T. R. (2002). Paleomagnetic results ror Columbia River basalts from west-central Idaho and the implications for the structural evolution of the Salmon River suture zone, paper no. 118-16. In *GSA 2002 Annual Meeting*. Denver, CO.

Kosterov, A. (2003). Low-temperature magnetization and AC susceptibility of magnetite: Effect of thermomagnetic history. *Geophysical Journal International*, *154*(1), 58–71. https://doi.org/10.1046/j.1365-246X.2003.01938.x

Lappe, S.-C. L. L., Bowles, J., Jackson, M., & Keavney, D. (2015). *XMCD and magnetic evidence for cation reordering in synthetic Mg- and Al-substituted titanomagnetites*, Abstract GP43A-1237. Paper presented at AGU Fall Meeting, San Francisco, CA.

Lattard, D., Engelmann, R., Kontny, A., & Sauerzapf, U. (2006). Curie temperatures of synthetic titanomagnetites in the Fe-Ti-O system: Effects of composition, crystal chemistry, and thermomagnetic methods. *Journal of Geophysical Research*, *111*, B12S28. https://doi.org/10.1029/2006JB004591

Lilova, K. I., Pearce, C. I., Gorski, C., Rosso, K. M., & Navrotsky, A. (2012). Thermodynamics of the magnetite-ulvospinel (Fe_3O_4-Fe_2TiO_4) solid solution. *American Mineralogist*, *97*(8-9), 1330–1338. https://doi.org/10.2138/am.2012.4076

Lindsley, D. H. (1977). Thermodynamic solution model for coexisting Ti-magnetite Plus ilmenite. *Eos, Transactions American Geophysical Union*, *58*, 519.

Lindsley, D. H. (1981). Some experiments pertaining to the magnetite-Ulvospinel miscibility gap. *American Mineralogist*, *66*(7–8), 759–762.

Melson, W. G., & Hopson, C. A. (1981). Preeruption temperatures and oxygen fugacities in the 1980 eruptive sequence. In P. W. Lipman & D. R. Mullineaux (Eds.), *The 1980 eruptions of Mount St. Helens* (Vol. 1250, pp. 641–648). Washington: USGS Professional Paper.

Merrill, R. T., & McElhinny, M. W. (1983). *The Earth's magnetic field: Its history, origin, and planetary perspective*, *International geophysics series* (Vol. 32, p. 401). Orlando, FL: Academic Press.

Moskowitz, B. M. (1985). Magnetic viscosity, diffusion after-effect, and disaccommodation in natural and synthetic samples. *Geophysical Journal of the Royal Astronomical Society*, *82*(2), 143–161. https://doi.org/10.1111/j.1365-246X.1985.tb05133.x

Moskowitz, B. M. (1987). Towards resolving the inconsistencies in characteristic physical-properties of synthetic titanomaghemites. *Physics of the Earth and Planetary Interiors*, *46*(1-3), 173–183. https://doi.org/10.1016/0031-9201(87)90180-4

Moskowitz, B. M., Jackson, M., & Kissel, C. (1998). Low-temperature magnetic behavior of titanomagnetites. *Earth and Planetary Science Letters*, *157*(3-4), 141–149. https://doi.org/10.1016/S0012-821X(98)00033-8

Mullins, C. E., & Tite, M. S. (1973). Magnetic viscosity, quadrature susceptibility, and frequency dependence of susceptibility in single-domain assemblies of magnetite and maghemite. *Journal of Geophysical Research*, *78*(5), 804–809. https://doi.org/10.1029/JB078i005p00804

Muxworthy, A. R. (1999). Low-temperature susceptibility and hysteresis of magnetite. *Earth and Planetary Science Letters*, *169*(1-2), 51–58. https://doi.org/10.1016/S0012-821X(99)00067-9

Muxworthy, A. R., & Williams, W. (2006). Observations of viscous magnetization in multidomain magnetite. *Journal of Geophysical Research*, *111*, B01103. https://doi.org/10.1029/2005JB003902

Néel, L. (1949). Théorie du traînage magnétique des ferromagnétiques en grains fins avec applications aux terres cuites. *Annales de Géophysique*, *5*, 99–136.

Néel, L. (1955). Some theoretical aspects of rock magnetism. *Advances in Physics*, *4*(14), 191–243. https://doi.org/10.1080/00018735500101204

O'Neill, H. S. C., & Navrotsky, A. (1984). Cation distributions and thermodynamic properties of binary spinel solid-solutions. *American Mineralogist*, *69*(7–8), 733–753.

O'Reilly, W. (1984). *Rock and mineral magnetism*. London: V., Blackie. https://doi.org/10.1007/978-1-4684-8468-7

O'Reilly, W., & Banerjee, S. K. (1965). Cation distribution in titanomagnetites $(1-x)\,Fe_3O_4-xFe_2TiO_4$. *Physics Letters*, *17*(3), 237–238. https://doi.org/10.1016/0031-9163(65)90504-4

Özdemir, Ö., & Dunlop, D. J. (2010). Hallmarks of maghemitization in low-temperature remanence cycling of partially oxidized magnetite nanoparticles. *Journal of Geophysical Research*, *115*, B02101. https://doi.org/10.1029/2009JB006756

Özdemir, Ö., Dunlop, D. J., & Jackson, M. (2009). Frequency and field dependent susceptibility of magnetite at low temperature. *Earth, Planets and Space*, *61*(1), 125–131. https://doi.org/10.1186/BF03352892

Paterson, G. A., Muxworthy, A. R., Roberts, A. P., & Mac Niocaill, C. (2010). Assessment of the usefulness of lithic clasts from pyroclastic deposits for paleointensity determination. *Journal of Geophysical Research*, *115*, B03104. https://doi.org/10.1029/2009JB006475

Paterson, G. A., Roberts, A. P., Mac Niocaill, C., Muxworthy, A. R., Gurioli, L., Viramonte, J. G., … Weider, S. (2010). Paleomagnetic determination of emplacement temperatures of pyroclastic deposits: An Under-utilized tool. *Bulletin of Volcanology*, *72*(3), 309–330. https://doi.org/10.1007/s00445-009-0324-4

Price, G. D. (1981). Diffusion in the titanomagnetite solid-solution series. *Mineralogical Magazine*, *44*(334), 195–200. https://doi.org/10.1180/minmag.1981.044.334.13

Price, G. D. (1982). Exsolution in titanomagnetites as an indicator of cooling rates. *Mineralogical Magazine*, *46*(338), 19–25. https://doi.org/10.1180/minmag.1982.046.338.04

Radhakrishnamurty, C., & Likhite, S. D. (1993). Frequency dependence of low-temperature susceptibility peak in some titanomagnetites. *Physics of the Earth and Planetary Interiors*, *76*(1-2), 131–135. https://doi.org/10.1016/0031-9201(93)90062-E

Readman, P. W., & O'Reilly, W. (1972). Magnetic properties of oxidized (cation-deficient) titanomagnetites (Fe, Ti, _??_)4_3O_4. *Journal of Geomagnetism and Geoelectricity*, *24*(1), 69–90. https://doi.org/10.5636/jgg.24.69

Rosenbaum, J. G. (1993). Magnetic grain-size variations through an ash-flow sheet: Influence on magnetic properties and implications for cooling history. *Journal of Geophysical Research*, *98*(B7), 11,715–11,727. https://doi.org/10.1029/93JB00355

Sauerzapf, U., Lattard, D., Burchard, M., & Engelmann, R. (2008). The titanomagnetite–ilmenite equilibrium: New experimental data and thermo-oxybarometric application to the crystallization of basic to intermediate rocks. *Journal of Petrology*, *49*(6), 1161–1185. https://doi.org/10.1093/petrology/egn021

Senderov, E., Dogan, A. U., & Navrotsky, A. (1993). Nonstoichiometry of magnetite-ulvospinel solid-solutions quenched From 1300°C. *American Mineralogist*, *78*(5–6), 565–573.

Shcherbakov, V. P., & Fabian, K. (2005). On the determination of magnetic grain-size distributions of superparamagnetic particle ensembles using the frequency dependence of susceptibility at different temperatures. *Geophysical Journal International*, *162*(3), 736–746. https://doi.org/10.1111/j.1365-246X.2005.02603.x

Skomski, R., & Sellmyer, D. J. (2000). Curie temperature of multiphase nanostructures. *Journal of Applied Physics*, *87*(9), 4756–4758. https://doi.org/10.1063/1.373149

Stephenson, A. (1969). The temperature dependent cation distribution in titanomagnetites. *Geophysical Journal of the Royal Astronomical Society*, *18*(2), 199–210. https://doi.org/10.1111/j.1365-246X.1969.tb03562.x

Stephenson, A. (1972a). Spontaneous magnetization curves and Curie points of cation deficient titanomagnetites. *Geophysical Journal of the Royal Astronomical Society*, *29*(1), 91–101. https://doi.org/10.1111/j.1365-246X.1972.tb06154.x

Stephenson, A. (1972b). Spontaneous magnetization curves and Curie points of spinels containing two types of magnetic iron. *Philosophical Magazine*, *25*(5), 1213–1232. https://doi.org/10.1080/14786437208226863

Trestman-Matts, A., Dorris, S. E., Kumarakrishnan, S., & Mason, T. O. (1983). Thermoelectric determination of cation distributions in Fe_3O_4-Fe_2TiO_4. *Journal of the American Ceramic Society*, *66*(12), 829–834. https://doi.org/10.1111/j.1151-2916.1983.tb10996.x

van Velzen, A. J., & Dekkers, M. J. (1999). Low-temperature oxidation of magnetite in loess-paleosol sequences: A correction of rock magnetic parameters. *Studia Geophysica et Geodaetica*, *43*(4), 357–375. https://doi.org/10.1023/A:1023278901491

Wadge, G., Voight, B., Sparks, R. S. J., Cole, P. D., Loughlin, S. C., & Robertson, R. E. A. (2014). An overview of eruption of Soufrière Hills volcano, Montserrat from 2000 to 2010. In G. Wadge, et al. (Eds.), *The eruption of Soufrière Hills volcano, Montserrat from 2000 to 2010* (Vol. 39, pp. 1–39). London: Geological Society.

Walz, F., Brabers, V. A. M., Brabers, J., & Kronmueller, H. (2007). Vacancy-interstitial annihilation in titanomagnetite by thermal annealing. *Physica Status Solidi (A)-Applications and Materials Science*, *204*(10), 3514–3525. https://doi.org/10.1002/pssa.200723005

Walz, F., Brabers, V. A. M., Brabers, J. H. V. J., & Kronmuller, H. (2003). Stress-induced relaxation mechanisms in single-crystalline titanomagnetites. *Journal of Physics: Condensed Matter*, *15*(41), 7029–7045.

Walz, F., & Kronmüller, H. (1994). Analysis of magnetic point-defect relaxations in electron-irradiated magnetite. *Physica Status Solidi B*, *181*(2), 485–498. https://doi.org/10.1002/pssb.2221810225

Walz, F., Torres, L., Bendimya, K., de Francisco, C., & Kronmueller, H. (1997). Analysis of magnetic After-effect spectra in titanium-doped magnetite. *Physica Status Solidi A*, *164*(2), 805–820. https://doi.org/10.1002/1521-396X(199712)164:2%3C805::AID-PSSA805%3E3.0.CO;2-N

Wanamaker, B. J., & Moskowitz, B. M. (1994). Effect of nonstoichiometry on the magnetic and electrical-properties of synthetic single-crystal $Fe_{2.4}Ti_{0.6}O_4$. *Geophysical Research Letters*, *21*(11), 983–986. https://doi.org/10.1029/94GL00877

Wechsler, B. A., Lindsley, D. H., & Prewitt, C. T. (1984). Crystal-structure and cation distribution in titanomagnetites ($Fe_{3-X}Ti_XO_4$). *American Mineralogist*, *69*(7–8), 754–770.

Wirth, K. R., Goodge, J., Perkins, D., & Stokes, A. (2011). An excursion to the classic bedrock localities of northeastern Minnesota with a focus on teaching and learning in the field. *GSA Field Guides*, *24*, 483–503. https://doi.org/10.1130/2011.0024(24)